Reliable before-fabrication forecasting of expected surface slope distributions for x-ray optics

Yekaterina V. Yashchuk[†] and Valeriy V. Yashchuk*

Lawrence Berkeley National Laboratory, Berkeley, California 94720

*Corresponding author: VVYashchuk@lbl.gov

[†] Currently at Esurance, Inc., San Francisco, California 94111

ABSTRACT

Numerical simulation of the performance of new beamlines and those under upgrade requires sophisticated and reliable information about the expected surface slope and height distributions of planned x-ray optics before they are fabricated. Obtaining such information should be based on the metrology data measured from existing mirrors that are made by the same vendor and technology; but, generally, with different sizes, slope and height rms variations. In this work, we demonstrate a method for highly reliable forecasting of the expected surface slope distributions of the prospective x-ray optics. The method is based on an autoregressive moving average (ARMA) modeling of the slope measurements with a limited number of parameters. With the found parameters of the ARMA model, the surface slope profile of an optic with the newly desired specification can reliably be forecast. We demonstrate the high accuracy of this type of forecasting by comparing the power spectral density distributions of the measured and forecast slope profiles.

Keywords: surface metrology, surface profilometer, auto-regressive moving average, ARMA models, power spectral density, calibration, fabrication tolerances, metrology of x-ray optics

1. INTRODUCTION

Development of new beamlines for third-generation synchrotron radiation sources and free electron lasers (FELs) relies on availability of x-ray optics of unprecedented quality with surface slope precision in the range of 0.1-0.2 μrad and surface height error of less than 1 nm.[1-5] During the last few years, significant progress on fabrication of such high quality x-ray optics has been achieved.[6-12] In addition to the new and sophisticated fabrication technologies, which have resulted in significant progress in optical fabrication, a new level of performance in beamlines has become possible due to the development of dedicated high accuracy metrology methods and techniques for surface characterization in the laboratory before installation.[13-27] The operational scope of this metrology is being extended to the tuning and alignment of the optics in situ.[28-34]

The uniqueness of the optics and the limited number of proficient vendors makes fabrication extremely time consuming and expensive. It is therefore essential to provide a specification for optical fabrication that is numerically evaluated to be adequate to the required beamline performance, avoiding over- as well as under-specification.

One of the most insightful approaches to evaluate the performance of X-ray optical systems consists of sophisticated X-ray scattering calculations based on the two-dimensional (2D) power spectral density (PSD) distribution of the surface height, allowing for the evaluation of three-dimensional distributions of X-rays scattered by the optics.[35-37] A comprehensive discussion of the importance of the characterization of highly finished optical surfaces via the PSD distribution can be found in Refs.[38,39]

Statistical description of surface topography via 1D and 2D PSD distributions is basically a spectral analysis of surface height measurements. It is used to parameterize, specify, and model the topography of optical and engineering components,[39-42] as well as fabrication technologies, including

optical polishing,[43] lithography,[44] surface coating and multilayer deposition.[45,46] Reliability of the PSD data for these and other applications depends on experimental methods available for comprehensive characterization and calibration of the spatial frequency response of the metrology instruments in use.[47-65] There are also problems inherent in the statistical description of surface metrology data that we discuss in the next section.

Another powerful approach to predict the performance of an optical system, in general, and a synchrotron radiation beamline, in particular, is the use of ray tracing methods.[66-72] Ray-tracing calculations allow evaluation of the effect of lower spatial frequency errors of optical surfaces usually given with residual (after subtraction of the desired surface shape) slope distributions.

For designing and optimizing synchrotron radiation beamlines, the ray-tracing code SHADOW[66,67] is extensively used. In the standard version of SHADOW,[66] the slope error is specified with a surface defined by a maximum of 200 points.[73] For a fabricated optic, this is straightforward when using a residual slope trace measured with a slope profiler. For simulating optical slope errors before the optic is available, a special method for introducing waviness effects of real and simulated optical surfaces in ray-tracing calculations is presented in Ref.[67] This method, fully integrated in the SHADOW environment, allows only for estimation of an effect of a single harmonic variation of surface figure. To the best of our knowledge, there are no methods for reliable prediction of surface slope errors of an optic before it is available that could be used as the input data for SHADOW simulation of the beamlines under design.

Therefore, the numerical simulation of the performance of new beamlines and those under upgrade requires refined and reliable information about the expected surface slope and height distributions of the planned x-ray optics before they are fabricated. Obtaining such information

should be based on the metrology data measured from existing mirrors that are made by the same vendor and technology, but, generally, with different sizes, slope and height rms variations.

In the present work, we demonstrate a method for highly reliable forecasting of the expected surface slope distributions of the prospective x-ray optics. The method is based on an autoregressive moving average (ARMA) modeling of surface slope metrology data obtained with existing optics fabricated by the same prospective vendor with the same technology. The best-fitted ARMA model has a limited number of parameters that can be determined with the use of standard statistical software. With the found parameters of the ARMA model, the surface slope profile of an optic with the newly desired specification can reliably be forecast. We demonstrate the high accuracy of this type of forecasting by comparing the power spectral density distributions of measured and forecast slope profiles.

This paper is organized as follows. In the next section, we discuss the problems of finding reliable PSD distributions by direct discrete Fourier transformation (DFT) of surface height and slope measurements. In Sec. 3, we briefly give the overview of the mathematical fundamentals of ARMA modeling of random rough surfaces. The results of ARMA fitting of the slope measurements with a high quality reference mirror are presented and discussed in Sec. 4. Section 5 describes an ARMA-modeling based method for forecasting of surface slope distributions of X-ray optics before fabrication. The paper concludes (Sec. 6) by summarizing the main concepts discussed throughout the paper and stating a plan for extending the suggested approach to parameterize polishing performances of different technologies available from a variety of vendors.

2. PROBLEMS OF FINDING RELAIBLE PSD DISTRIBUTIONS FROM MEASUREMENTS OF SURFACE HEIGHT AND SLOPE DISTRIBUTIONS

In the early 1990's, Church and Takacs pointed out that the specification of surface figure and finish of X-ray mirrors must be based on their imaging performance and the results must be expressed in term of statistical quantities (rms roughness and residual slope variation) that are directly accessible from optical metrology.[74,75] This suggests that a spatial frequency bandwidth for the estimation of surface errors must be determined by the beamline system parameters rather than by the metrology instruments. Practically, in order to estimate the error parameters over the bandwidth related to the system performance, the PSD spectra measured with bandwidth-limited instruments are extrapolated to the wanted frequency range by fitting a more or less simple analytical model, such as an inverse-power-law (fractal, if power between 1 and 3) spectral distribution.[76,77] The PSD extrapolation is more reliable when based on PSD measurements performed with different instruments providing different but, preferably, overlapping spatial frequency ranges.[56-58,78,79] Accordingly, the found extrapolated (modeled) PSD spectrum is used (via inverse Fourier transform) for the simulation of metrology data for X-ray optics before fabrication and prediction of the performance of the optical system.[39-42]

PSD based forecasting works rather well for prediction of expected surface height distributions in the medium spatial frequency range approximately between 10^{-3} and 1 μm^{-1} available with optical interferometric microscopes.[56-58] In this case, 1D PSD spectra of many high quality x-ray optics can be approximated by an inverse-power-law function A/f^{γ} with a power parameter $\gamma \approx 1$.[57,74,75,80]

For lower spatial frequencies, accessible for surface height measurements, for example, with large field-of-view Fizeau interferometers, the measured PSD spectra were found to be well approximated by an inverse-power-law function with a significantly larger power parameter,

typically $\gamma \approx 2$.[57,74,75] This can occur as a result of normal polishing processes, where the surface starts out as a rough surface and then becomes smoother by knocking down the high frequency end of the spectrum faster than the low end. It also can be due to instrumental noise and/or data processing (detrending, windowing).[78] Indeed, as shown in Ref.[57] for a stainless steel mirror, tangential 1D PSD spectra, extracted from ZYGO™ GPI measurements, strongly depend on applied detrending performed either by subtracting the piston and the tilt from the corresponding height distributions, or by subtracting the best-fitted second power polynomial function. Moreover, the result of detrending strongly depends on the size of the area used for the fitting.

The detrending problem is closely related to a general problem of spectral analysis known as the problem of statistical stability of data. A reliable PSD estimation based on a limited number of observations can only be obtained for a wide sense stationary (WSS) random process (see, for example, Ref.[81]). The process $h[n]$, where $n = 1,..,N$, N being the number of observations, is a WSS process if its autocorrelation function (ACF),

$$r_h[l] = E(h[n]h[n-l]), \tag{1}$$

depends only on the lag l, and does not depend on the value of n. In (1) E is the expectation operator. Note that the PSD of the WSS random process $h[n]$ can be found from the ACF:

$$P_h(f) = \sum_{l=-\infty}^{\infty} r_h[l] e^{-i2lf} . \tag{2}$$

Therefore, dependence of the detrended surface on the number of observations (size of the fitted area) can be thought of as a signature for a potential statistical instability of the data.

Obtaining reliable PSD spectra from surface slope measurements appears to be more trustworthy. According to the derivative theorem of the Fourier transform, the PSD of surface slope

distribution, $P_\alpha(f)$, and PSD obtained from the corresponding height measurement, $P_h(f)$, are related as the following function,

$$P_\alpha(f) = (2\pi f)^2 P_h(f). \tag{3}$$

Therefore, in the slope domain, the detrending problem is less important; and the PSD spectra extracted from slope measurements are expected to be more reliable.

Note that according to its definition (2), the PSD depends on an infinite number of ACF values, which means that the determination of PSD is in general an impossible task. For a single limited realization, one can only make an estimation of the PSD. Generally, the estimated PSD spectrum has very poor statistical stability seen as intense fluctuation from frequency to frequency and from realization to realization. The same result is usually obtained for the PSD spectrum straightforwardly estimated via the squared Fourier coefficients derived from a particular realization, as described, e.g., in Refs.[56-58] (see also Sec. 3).

The statistical stability of the resulting PSD spectrum can be improved by averaging over the PSDs of a number of uncorrelated measurements performed with unchanged conditions. Averaging is usually possible for medium spatial frequency PSDs. In this case, surface profiles measured over a number of significantly separated sub-areas are statistically uncorrelated; and averaging over the corresponding PSDs suppresses the spectral fluctuations.

In the case of lower spatial frequency PSD measurements with X-ray optics, measurements are performed over the entire optical clear aperture. Therefore, statistically uncorrelated measurements can only be made with different optics fabricated with the same technology. This is usually impossible because of the uniqueness of the optics.

In addition to the problem of statistical stability, one should consider possible perturbation of PSD measurements by air convection that is one of the most prominent sources of errors in optical slope measurements.[82] The characteristic spectrum of the air convection noise, is approximately described by a random distribution at lower frequencies, ≤ 0.1 Hz, and an inverse-power-law function with a power parameter close to one at higher frequencies.[82] Because of their sequential, point-by-point nature, these slope measurements are usually slow enough to make air convection noise appear as a white noise.

On account of relation (3), a similar behavior of the air convection noise is also characteristic of interferometric measurements,[83] and leads to a significantly larger perturbation of the PSD in the height domain than in the slope domain.

Concluding this section, we refer to classical work[36] by Church and Berry, where a comprehensive analysis of the problems and the limitations of reliable spectral estimations of measured surface profile data, is provided. The work also discusses a possibility to treat the random rough surface as the result of a stochastic random process described by an autoregressive (AR) model.[81,84] The surface description based on the AR model or the extended ARMA model provides a way to replace the spectral estimation problem by that of parameter estimation.

3. ARMA MODELING OF RANDOM ROUGH SURFACES

For a one dimensional case, ARMA modeling of a random rough surface consists of describing the discrete surface height distribution $h[n]$, measured uniformly, with an increment Δx, distributed points of a trace $x_n = n \cdot \Delta x$ [where $n = 1, ..., N$ and $(N-1)\Delta x$ is the total length of the trace], as a result of a stochastic process:[81,84]

$$h[n] = \sum_{l=1}^{p} a_l h[n-l] + \sum_{l=0}^{q} b_l v[n-l], \tag{4}$$

where $\nu[n]$ is the zero mean unit variance white Gaussian noise that is the driving noise of the model. Parameters p and q are the orders of the autoregressive and moving average processes, respectively. At $q=0$ and $b_0=1$, the ARMA process (4) reduces to an AR stochastic process. The goal of the fitting is to determine the ARMA orders and estimate the corresponding AR and MA coefficients a_l and b_l.[85-87] Due to the development of sophisticated statistical software capable for ARMA analysis of experimental data, such fitting is quiet a routine task (see Sec. 4).

ARMA fitting allows for the replacement of the spectral estimation problem by a problem of parameter estimation. In principle, the parameters of a successful ARMA model of a rough surface should relate to the polishing process. The analytical derivation of such relation is a separate and difficult task; there are just a few works that attempt to solve the problem.[43,88] Instead, most of the existing work provides an empirical ARMA description of the results of the polishing processes.[85,89] When an ARMA model is identified, the corresponding PSD distribution can be analytically derived:[81]

$$P_h(f)=\sigma^2\frac{B[e^{i2\pi f}]B[e^{-i2\pi f}]}{A[e^{i2\pi f}]A[e^{-i2\pi f}]}=\sigma^2\sum_{l=-\infty}^{\infty}r_h[l]e^{-i2\pi l f}\ , \tag{5}$$

where the frequency $f\in[-0.5,0.5]$,

$$A[e^{i2\pi f}]=1+a_1e^{i2\pi f}+\ldots+a_pe^{i2\pi p f}\ , \tag{6}$$

$$B[e^{i2\pi f}]=b_0+b_1e^{i2\pi f}+\ldots+b_qe^{i2\pi q f}\ , \tag{7}$$

and the ACF of the surface profile is determined by Eq. (1). Equation (5) can be expressed as

$$P_x(f)=\sigma^2\frac{(b_0+b_1z^{-1}+\ldots+b_qz^{-q})(b_0+b_1z^{1}+\ldots+b_qz^{q})}{(1-a_1z^{-1}-\ldots-a_pz^{-p})(1-a_1z^{1}-\ldots-a_pz^{p})}=\sigma^2\sum_{l=-\infty}^{\infty}r_h[l]z^{-l}\ , \tag{8}$$

where $z = e^{i2\pi q f}$, and σ^2 is the variance of the driving noise $\nu[n]$. According to Eq. (8), $r_h[l]$ is a nonlinear function of the ARMA coefficients, a_l for $l = 1,..., p$ and b_l for $l = 1,..., q$.

Therefore, a low-order ARMA fit, if successful, allows parameterization of both the PSD and the ACF of a random rough surface. As a result, the PSD distributions appear as highly smoothed versions of the corresponding estimates via a direct DFT. Description of a rough surface as the result of an ARMA stochastic process provides a model-based mechanism for extrapolating the spectra outside the measured bandwidth[90-93] (see also Sec. 5).

Below, we demonstrate successful application of ARMA modeling to surface slope data.

4. ARMA FITTING OF SLOPE MEASUREMENTS WITH A HIGH QUALITY OPTIC

As mentioned before, due to the availability of sophisticated statistical software capable for ARMA modeling of experimental data, ARMA fitting becomes a rather routine task of finding the ARMA model parameters and verifying the statistical reliability of the model. In the present work, we use a commercially available software package EViews 7.[94] In particular, the software provides easy-to-use ARMA modeling tools oriented to econometric analysis, forecasting, and simulation.

Throughout the present work, we use experimental surface slope data for a 1280 m radius spherical reference mirror,[95,96] obtained with the Advanced Light Source (ALS) Developmental Long Trace Profiler (DLTP).[27] The major reason for the selection of this data is its very high accuracy with a low contribution from random and systematic errors. The accuracy of the data has been verified by cross-comparison with measurements performed with the HZB/BESSY-II Nanometer Optical Component Measuring machine (NOM),[14-16] one of the world's best slope measuring instruments. The difference of the NOM and DLTP measurements does not exceed ±0.15 μrad; the rms variation of the difference is 86 nrad.

Figure 1a reproduces the measured slope trace (the solid blue line) after subtracting the best-fit spherical surface shape with a radius of curvature of 1287.5 m. The trace consists of N=547 points measured with an increment of $\Delta x = 0.2$ mm.

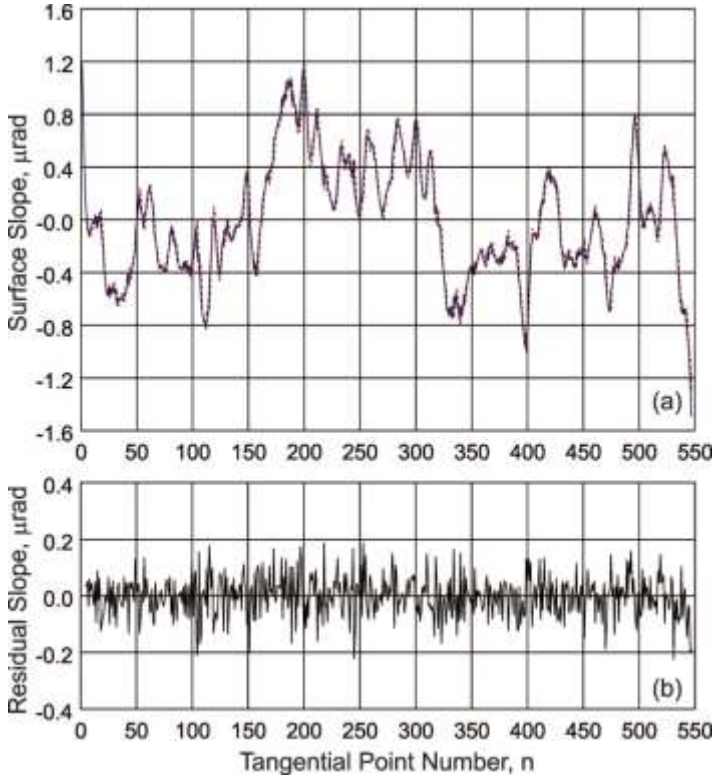

Figure 1. (a) Measured slope trace after subtracting the best-fitted spherical surface shape with a radius of curvature of 1287.5 m (the solid blue line); and best-fitted slope trace corresponding to the ARMA model specified in Table 1 (the red dashed line). The rms variation of the measured slope trace is 0.447 µrad. (b) Residual slopes equal to the difference between the measured and fitted traces in plots (a). The rms variation of the residual slope trace is 0.073 µrad. Note that the measured and the best-fitted traces are almost exactly overlapping.

The best fitted slope trace, shown in Fig. 1a with the red dashed line, corresponds to the ARMA model specified in Table 1. The table, generated by EViews 7 software as the regression output, only includes the statistically significant ARMA parameters. As can be seen by the low probabilities and the high t-statistics in the regression outputs (Table 1), the AR(1), AR(4), MA(2), MA(6), and MA(3) coefficients are highly significant at <1% significance level.

Table 1. Parameters of the ARMA model (the red dashed line in Fig. 1a), which best fits the surface slope trace for the 1280 m radius spherical reference mirror measured with the ALS DLTP.[27] In Eqs. (4-8), $b_0 = 1$ and σ^2 is equal to the standard error (S.E.) of the regression. The data in the table are the regression outputs generated by EViews 7 software.

Dependent Variable: SLOPE
Method: Least Squares
Included observations: 543 after adjustments
Convergence achieved after 6 iterations

Variable	Coefficient	Std. Error	t-Statistic	Prob.
AR(1): a_1	1.118736	0.021838	51.22914	0.0000
AR(4): a_4	-0.145061	0.022404	-6.474687	0.0000
MA(2): b_2	0.299157	0.035204	8.497827	0.0000
MA(6): b_6	-0.171479	0.036455	-4.703891	0.0000
MA(3): b_3	0.093133	0.032904	2.830432	0.0048

R-squared	0.973238	Mean dependent variation	-0.016092
Adjusted R-squared	0.973039	S.D. dependent variation	0.443422
S.E. of regression	0.072809	Akaike info criterion	-2.392786
Sum squared residuals	2.852027	Schwarz criterion	-2.353218
Log likelihood	654.6415	Hannan-Quinn criterion	-2.377315
Durbin-Watson statistics	2.068010		

The regression output, generated by EViews software (Table 1), contains the results of the application of several methods helpful for evaluation of the reliability of the regression. $R^2 \approx 0.97$

indicates that the regression describes 97% of the data's variance. The Durbin-Watson statistic, a test for first order serial correlation of the residuals, is around 2, suggesting that there is no serial correlation. EViews also reports various informational criteria that are helpful as a model selection guide, for example, when examining the number of regression lags.[81,94]

The residual slope trace shown in Fig. 1b is the driving noise of the model $v[n]$ in Eq. (4) and should be distinguished from any observation noise. According to the ARMA definition, the driving noise must be normally distributed. Figure 2 reproduces the results of EViews' normality test for the residuals. Together with other criteria, the low Jarque-Bera statistic[94] and the high probability indicate that the residuals are normally distributed.

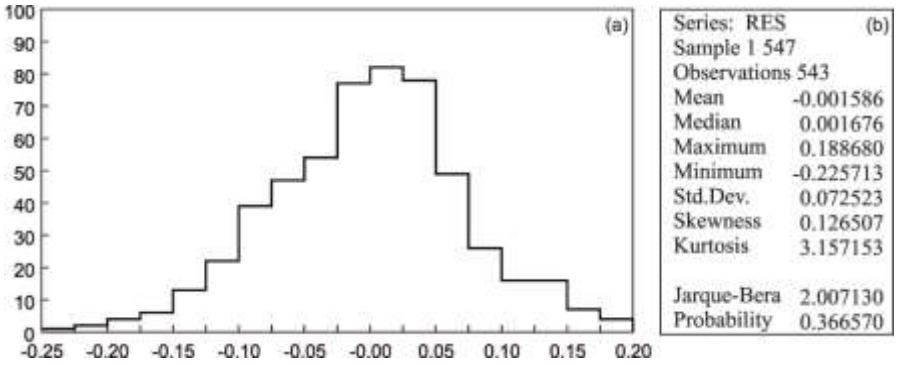

Figure 2. Histogram normality test[94] for the residual slope of the regression shown in Fig. 1. (a) Histogram of the residuals. (b) Descriptive statistics of the residuals, including the Jarque-Bera statistic used for testing whether the residuals are normally distributed. All the descriptive statistics indicate that the residual slope is normally distributed.

Figure 3 represents the PSD distributions of the measured and fitted slope traces shown in Fig. 1. The PSDs are directly calculated via the discrete Fourier transform (see, for example, Refs.[56-58]):

$$P_{DFT}(f) = \Delta x \cdot \left| F[h(x_n)] \right|^2 . \quad (9)$$

The normalization coefficient in Eq. (9) depends on the definition of the discrete Fourier transform applied. The normalization, used here, corresponds to the Mathematica™ default definition of the DFT.

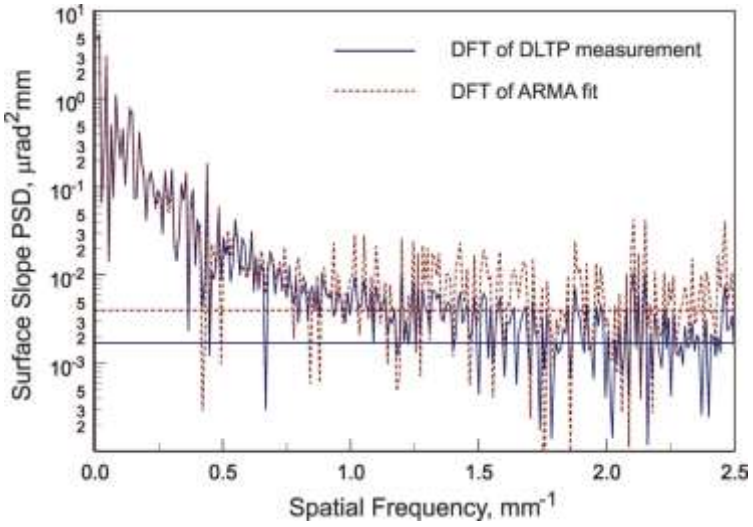

Figure 3. Power spectral density distributions of the measured slope data (the solid blue curve) and the best-fitted ARMA model of the data (the dashed red curve). The corresponding straight lines depict the white-noise asymptotical behavior of the PSD distributions at the higher spatial frequencies.

The blue solid straight line in Fig. 3 marks the asymptotical behavior of the measured PSD distribution at the higher spatial frequencies (≥1.7 mm^{-1}), where the PSD looks like white noise with a constant level of 0.017 $\mu rad^2 \cdot mm$. For the measured spatial frequency range, the white noise PSD of 0.017 $\mu rad^2 \cdot mm$ corresponds to the rms slope variation of approximately 0.065 μrad. That value is in good agreement with the expected random noise of the DLTP due to air convection. The frequency limit of 1.7 mm^{-1} can relate to the instrumental resolution that is basically unknown and

can only be roughly estimated from the spot size of the DLTP light beam of 2.5 mm diameter.[16] The tangential position increment of 0.2 mm, used for the measurements, suggests significant oversampling. Nevertheless, the oversampling can be justified as necessary for superior matching of the ALS and the BESSY measurements when cross-checking.

The ARMA model perfectly fits the measured spectrum at the lower and middle spatial frequencies. This range covers the entire bandwidth of the DLTP at the current resolution. The asymptotical white noise level of the ARMA best-fit model, shown in Fig. 3 with the red dotted straight line, is higher, about 0.04 $\mu rad^2 \cdot mm$. The corresponding rms variation is approximately 0.1 μrad. This is the result of the combined variance of the random noise of the measurement and the driving residuals of the ARMA model. Here we ignore the increase of the noise level and do not consider the questions of ARMA fitting in the presence of noticeable measurement noise.[97,98]

As expected for a single limited realization of the slope profile and, in turn, a single ARMA model of the profile, the PSD distributions in Fig. 3 have rather poor statistical stability. This is seen as an intense frequency-to-frequency fluctuation of the spectra.

The result of the direct analytical calculation of the PSD of the best-fitted ARMA model is shown in Fig. 4 with the bold solid curve. The calculation was performed using expression (9) with ARMA parameters from Table 1 and $\sigma^2 = 0.072809^2$. Over the entire bandwidth of the measurement, the ARMA analytical PSD precisely fits the noisy PSD spectrum obtained by the DFT of the measured slope data.

In order to understand the stability of the ARMA PSD estimation, we also calculated two ARMA predictions with the modified ARMA parameters. In Fig. 4, the dotted line depicts the ARMA analytical PSD, calculated with the parameters from Table 1 increased by their standard errors; while the dashed line corresponds to the same parameters but decreased by the standard errors. The

upper extreme prediction is very close to the least-squares-method result; while the lower one is significantly shifted downwards at lower spatial frequencies. This naturally reflects the poor statistical confidence of the measurement at the lower spatial frequencies. As a whole, the statistical stability of the ARMA analytical PSD is significantly higher than that of the DFT PSD spectrum.

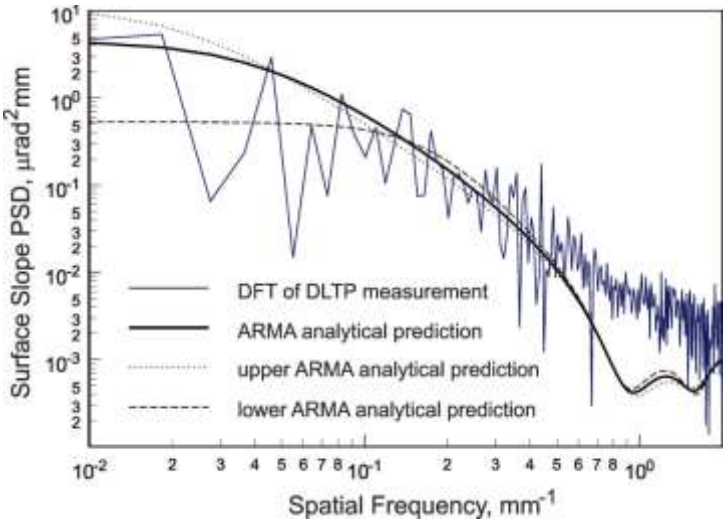

Figure 4. ARMA analytical PSD calculated with the parameters given in Table 1 (the bold solid line) and two extreme ARMA predictions with increased (the dotted line) and decreased (the dashed line) ARMA parameters; see text for details. For comparison, the DFT PSD spectrum of the measured slope trace is also shown with the solid blue curved line.

The only visual discrepancy between the measured DFT PSD and the PSD that was analytically derived for the ARMA model is seen at the higher spatial frequency end of the spectrum. In spite of the fact that the discrepancy is outside of the instrumental bandwidth, its appearance should be explained. Currently we do not have a solid understanding of this. The most probable origin of the discrepancy is due to the instrumental noise. Another possibility can be related to the sensitivity of

the ARMA fitting to data oversampling, which was mentioned above. It can also be that the ARMA modeling with a limited number of ARMA terms does not describe the data at the higher spatial frequencies. It also can be that the measured data are not perfectly described as a stationary (WSS) random process. There are statistical methods specially developed for reliable ARMA modeling of such data (see, for example, Ref.[99]). However, the discussion of these methods is out of the scope of this article.

In conclusion, the identified ARMA model, which included the AR(1), AR(4), MA(2), MA(6), and MA(3) terms, describes the actual slope data very well. To the best of our knowledge, this is the first demonstration that the autoregressive and moving average functions allow an analytical fit of metrology surface slope data and, therefore, parameterize the polishing process in the slope domain.

5. ARMA FORECASTING OF X-RAY OPTICS BEFORE FABRICATION

ARMA modeling of existing metrology data provides a natural approach for forecasting the quality of new optics before fabrication. The forecasting is based on the assumption that a certain polishing process at a particular fabrication facility is uniquely parameterized with its ARMA model. The question of uniqueness is out of the scope of this article. We plan to investigate the question by cross-comparing the ARMA models for different optics that are identically fabricated.

Technically, forecasting based on ARMA modeling can be performed in a few different ways depending on the task and the characteristics of the available metrology data.

The simplest task is to forecast a prospective optic that differs from the measured one only by increased length. In this case, the ARMA driving residuals can be extended to the required length by using a white noise generator. The generated white noise residuals must be renormalized in order to match the variance, σ^2, of the ARMA residuals. By using Eq. (4) with the found ARMA parameters and the extended residuals, an optic with the required length can be forecast. As for the length of that

of the measured optic, the forecast surface will have absolutely the same profile as the measured one. The profile of the forecast part of the optic will depend on the particular white noise realization used to extend the ARMA residuals.

For scattering and ray-tracing calculations, a number of statistically independent forecasts are usually desired. In this case, uncorrelated sets of white-noise-like residuals (over the entire profile length) can be generated with an appropriate variance. After that, statistically identical but uncorrelated optics would be forecast by using Eq. (4) with the pre-determined ARMA parameters and the generated sets of driving residuals.

Note that in both of these approaches, in order to reliably use the residuals generated with the white noise distribution, one should be sure that the ARMA residuals calculated by regression are normally distributed.

Figure 5a reproduces a slope trace of 1000 points (the blue solid line) generated with an ARMA model using the parameters given in the Table 1. The statistical behavior of the trace is similar to that of the surface slope trace of the 1280 m radius spherical reference mirror shown in Fig. 1. As the driving residuals, we used a white noise trace with a total number of 1000 points generated with EViews 7 software. The obtained white noise was renormalized in order to correspond to the desired rms variation of the forecast slope trace of 0.447 μrad.

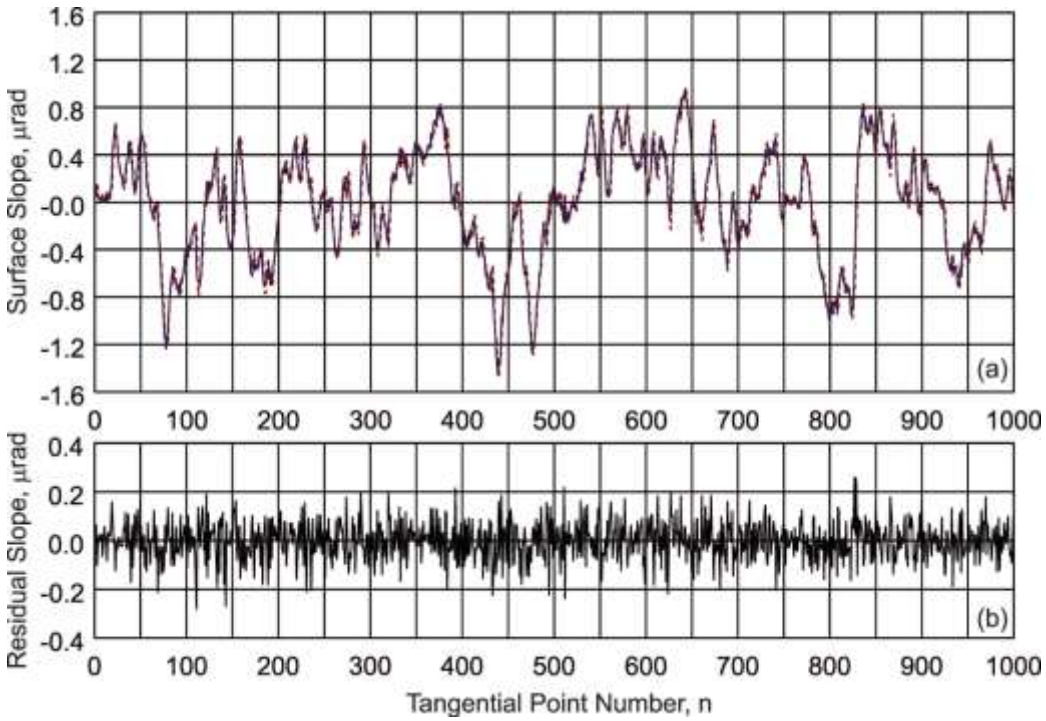

Figure 5. (a) Generated slope trace of 1000 points (the blue solid line) and the best-fitted slope trace (the red dashed line) corresponding to the ARMA model specified in Table 2. The rms variation of the generated slope trace of 0.447 µrad corresponds to the surface slope trace of the 1280 m radius spherical reference mirror (Fig. 1a). (b) Generated ARMA residuals with total number of 1000 points. The rms variation of the residual slope trace is 0.081 µrad. Note that the generated and the best-fitted traces are almost exactly overlapping.

In order to confirm the statistical reliability of the forecast, the generated slope trace was modeled with EViews 7 in a similar manner to the one described in Sec. 3. The fitted trace is shown in Fig. 5a with the red dashed line. The parameters of the ARMA model identified for the generated slope trace are presented in Table 2. Within the statistical uncertainty, the parameters are equal to those of the ARMA model of the measured slope trace (see Table 1).

Figure 6 presents the result (shown with the red bold curve) of the direct analytical calculation of the PSD of the generated slope trace. The calculation used expression (9) with the ARMA parameters from Table 2 and $\sigma^2 = 0.080981^2$. The blue solid line in Fig. 6 shows the corresponding DFT PSD distribution. Note, that the DFT PSD and the analytically calculated PSD in Fig. 6 were constructed assuming a tangential position increment of 0.2 mm, as used for the actual measurement.

The ARMA analytical PSD distribution perfectly fits the noisy PSD spectrum obtained by the DFT of the generated slope data. Unlike the measured data (Sec. 4), the agreement between the distributions is observed for the entire spatial frequency range.

Table 2. Parameters of the ARMA model (the red dashed line in Fig. 5a) found for the generated slope trace. The generated trace is statistically identical to the surface slope trace measured with the 1280 m radius spherical reference mirror and discussed in Sec. 3. The data in the table are the regression outputs generated by EViews 7 software.

Dependent Variable: GSLOPE
Method: Least Squares
Included observations: 996 after adjustments
Convergence achieved after 5 iterations

Variable	Coefficient	Std. Error	t-Statistic	Prob.
AR(1): a_1	1.048968	0.018116	57.90297	0.0000
AR(4): a_4	-0.085087	0.018392	-4.626384	0.0000
MA(2): b_2	0.349078	0.026168	13.33998	0.0000
MA(6): b_6	-0.179654	0.025161	-7.140075	0.0000
MA(3): b_3	0.114945	0.022912	5.016748	0.0000

R-squared	0.967377	Mean dependent variation	-0.067029
Adjusted R-squared	0.967245	S.D. dependent variation	0.447451
S.E. of regression	0.080981	Akaike info criterion	-2.184192
Sum squared residuals	6.498934	Schwarz criterion	-2.159575
Log likelihood	1092.728	Hannan-Quinn criterion	-2.174834
Durbin-Watson statistics	2.015141		

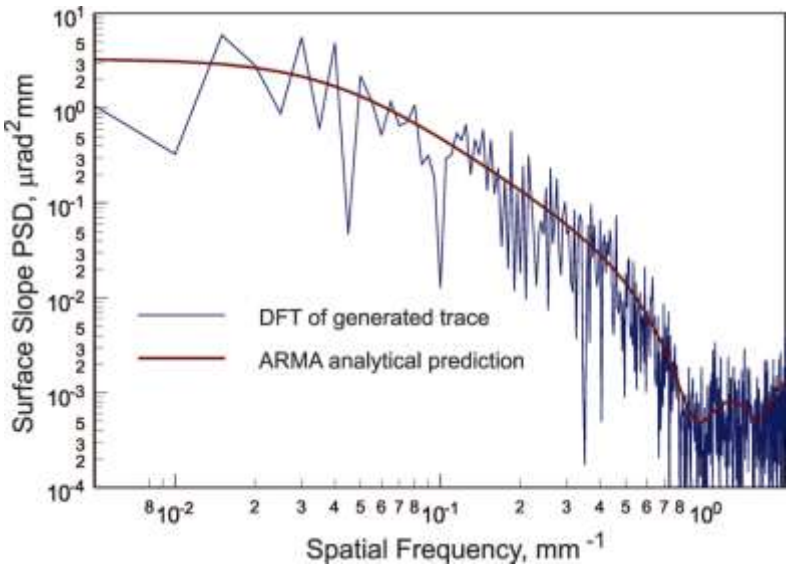

Figure 6. DFT PSD spectrum of the generated slope trace (the blue solid curved line) and the ARMA analytical PSD calculated with the parameters given in Table 2 (the red bold solid line).

6. CONCLUSION

At the ALS, we have started a new project that potentially will allow us to analytically characterize/parameterize polishing capabilities of different vendors for x-ray optics. Based on this parameterization, the expected surface profile of the perspective x-ray optics will be reliably simulated prior to purchasing new x-ray optics. The simulated profiles are also to be used for reliable estimations of the expected performance of the optics on the ALS beamlines prior to purchasing.

As the first step, we have investigated an application of the ARMA-modeling-based method to reliably forecast the expected surface slope distributions of the prospective x-ray optics. In this method, surface slope metrology data are first fitted to find the parameters of the suitable ARMA model. We assume that the parameters uniquely parameterize the corresponding fabrication

(polishing) technology available with a particular vendor. With the parameters of the ARMA model, the surface slope profile of an optic with a newly desired specification can been simulated. We have demonstrated the high applicability of this type of forecasting by comparing the power spectral density distributions of measured and forecast slope profiles.

The performed work has also raised a number of questions to be addressed in forthcoming investigations.

The major question is about the uniqueness of the ARMA parameterization for a certain polishing process. We plan to address this question by cross-comparing ARMA models from different optics which are identically fabricated. Archived metrology data for high quality x-ray optics, collected at the synchrotron facilities around the world, can be used.

Two-dimensional ARMA modeling is also possible using recent developments in the field of image and signal processing applications (see, for example, Ref.[100] and references therein).

ACKNOWLEDGEMENT

The authors are grateful to Howard Padmore and Wayne McKinney for useful discussions. The Advanced Light Source is supported by the Director, Office of Science, Office of Basic Energy Sciences, Material Science Division, of the U.S. Department of Energy under Contract No. DE-AC02-05CH11231 at Lawrence Berkeley National Laboratory.

commercial product, process, or service by its trade name, trademark, manufacturer, or otherwise, does not necessarily constitute or imply its endorsement, recommendation, or favoring by the United States Government or any agency thereof, or The Regents of the University of California. The views and opinions of authors expressed herein do not necessarily state or reflect those of the United States Government or any agency thereof or The Regents of the University of California.

REFERENCES

1. L. Assoufid, O. Hignette, M. Howells, S. Irick, H. Lammert, and P. Takacs, "Future metrology needs for synchrotron radiation grazing-incidence optics," *Nucl. Instrum. Methods* A **467-468**, 267-70 (2001).
2. K. Yamauchi, K. Yumamura, H. Mimura, Y. Sano, A. Saito, M. Kanaoka, K. Endo, A. Souvorov, M. Yabashi, K. Tamasaku, Y. Ishikawa, Y. Mori, "Wave-optical analysis of sub-micron focusing of hard x-ray beams by reflective optics," *Proc. SPIE* **4782**, 271-276 (2002).
3. N. Kelez, Y.-D. Chuang, A. Smith-Baumann, K. Franck, R. Duarte, A. Lanzara, M. Z. Hasan, D. S. Dessau, T. C. Chiang, Z.-X. Shen, Z. Hussain, "Design of an elliptically bent refocus mirror for the MERLIN beamline at the advanced light source," *Nucl. Instrum. Methods* A **582**(1), 135-137 (2007).
4. L. Samoylova, H. Sinn, F. Siewert, H. Mimura, K. Yamauchi, T. Tschentscher, "Requirements on Hard X-ray Grazing Incidence Optics for European XFEL: Analysis and Simulation of Wavefront Transformations," *Proc. SPIE* **7360**, 73600E (2009).
5. S. Moeller, J. Arthur, A. Brachmann, R. Coffee, F.-J. Decker, Y. Ding, D. Dowell, S. Edstrom, P. Emma, Y. Feng, A. Fisher, J. Frisch, J. Galayda, S. Gilevich, J. Hastings, G. Hays, P. Hering, Z. Huang, R. Iverson, J. Krzywinski, S. Lewis, H. Loos, M. Messerschmidt, A. Miahnahri, H.-D. Nuhn, D. Ratner, J. Rzepiela, D. Schultz, T. Smith, P. Stefan, H. Tompkins,

J. Turner, J. Welch, B. White, J. Wu, G. Yocky, R. Bionta, E. Ables, B. Abraham, C. Gardener, K. Fong, S. Friedrich, S. Hau-Riege, K. Kishiyama, T. McCarville, D. McMahon, M. McKernan, L. Ott, M. Pivovaroff, J. Robinson, D. Ryutov, S. Shen, R. Soufli, and G. Pile, "Photon beamlines and diagnostics at LCLS," *Nucl. Instrum. Methods* A **635**(1-1S) S6-S11 (2011).

6. K. Yamauchi, H. Mimura, K. Inagaki, and Y. Mori, "Figuring with sub-nanometer-level accuracy by numerically controlled elastic emission machining," *Rev. Sci. Instrum.* **73**(11), 4028-4033 (2002).
7. C. Liu, R. Conley, L. Assoufid, Z. Cai, J. Qian, and A. T. Macrander, "From flat substrate to elliptical KB mirror by profile coating," *AIP Conf. Proc.* **705**, 704-707 (2004).
8. F. Siewert, H. Lammert, T. Noll, T. Schlegel, T. Zeschke, T. Hänsel, A. Nickel, A. Schindler, B. Grubert, C. Schlewitt, "Advanced metrology: an essential support for the surface finishing of high performance x-ray optics," *Proc. SPIE* **5921**, 5921-01 (2005).
9. A. Schindler, T. Haensel, A. Nickel, H.J. Thomas, H. Lammert, F. Siewert, "Finishing procedure for high performance synchrotron optics," *Proc. SPIE* **5180**, 64-72 (2003).
10. M. Kanaoka, C. Liu, K. Nomura, M. Ando, H. Takino, Y. Fukuda, H. Mimura, K. Yamauchi, and Y. Mori, "Figuring and smoothing capabilities of elastic emission machining for low-thermal-expansion glass optics*," J. Vac. Sci. Technol.* B **25**(6) 2110-2113 (2007).
11. T. Arnold, G. Boehm, R. Fechner, J. Meister, A. Nickel, F. Frost, T. Haensel, A. Schindler, "Ultra-precision surface finishing by ion beam and plasma jet techniques: status and outlook," *Nucl. Instrum. Methods* A **616**, 147-156 (2010).
12. H. Thiess, H. Lasser, F. Siewert, "Fabrication of X-ray mirrors for synchrotron applications," *Nucl. Instrum. Methods* A **616**, 157–161 (2010).

13. P. Z. Takacs, "X-ray optics metrology," Chap. 46 in *Handbook of Optics*, 3rd ed., Vol. V, pp. 46.1-46.15, M. Bass, Ed., McGraw-Hill, New York (2009).

14. F. Siewert, T. Noll, T. Schlegel, T. Zeschke, and H. Lammert, "The Nanometer Optical Component Measuring machine: a new Sub-nm Topography Measuring Device for X-ray Optics at BESSY," *AIP Conf. Proc.* **705**, 847-850 (2004).

15. F. Siewert, H. Lammert, T. Zeschke, "The Nanometer Optical Component Measuring Machine;" Chap. 11 in *Modern Developments in X-Ray and Neutron Optics*, A. Erko, M. Idir, T. Krist, and A. G. Michette, Eds., pp. 193-200, Springer, New York (2008).

16. F. Siewert, J. Buchheim, and T. Zeschke, "Characterization and calibration of 2nd generation slope measuring profiler," *Nucl. Instrum. Methods* A **616**(2-3), 119-127 (2010).

17. R. D. Geckeler, I. Weingärtner, "Sub-nm topography measurement by deflectometry: flatness standard and wafer nanotopography," *Proc. SPIE* **4779,** 1-12 (2002).

18. R. D. Geckeler, "ESAD Shearing Deflectometry: Potentials for Synchrotron Beamline Metrology," *Proc. SPIE* **6317**, 63171H (2006).

19. H. Mimura, H. Yumoto, S. Matsuyama, K. Yamamura, Y. Sano, K. Ueno, K. Endo, Y. Mori, M. Yabashi, K. Tamasaku, Y. Nishino, T. Ishikawa, and K. Yamauchi, "Relative angle determinable stitching interferometry for hard x-ray reflective optics," *Rev. Sci. Instrum.* **76**, 045102 (2005).

20. H. Yumoto, H. Mimura, S. Handa, T. Kimura, S. Matsuyama, Y. Sano, H. Ohashi, K. Yamauchi, and T. Ishikawa, "Stitching-angle measurable microscopic-interferometer: Surface-figure metrology tool for hard X-ray nanofocusing mirrors with large curvature," *Nucl. Instrum. Methods* A **616**(2-3), 203-206 (2010).

21. S. G. Alcock, K. J. S. Sawhney, S. Scott, U. Pedersen, R. Walton, F. Siewert, T. Zeschke, F. Senf, T. Noll and H. Lammert, "The Diamond-NOM: A non-contact profiler capable of characterizing optical figure error with sub-nanometre repeatability," *Nucl. Inst. Methods* A **616**(2-3), 224-228 (2010).

22. Y. Senba, H. Kishimoto, H. Ohashi, H. Yumoto, T. Zeschke, F. Siewert, S. Goto, T. Ishikawa, "Upgrade of long trace profiler for characterization of high-precision X-ray mirrors at SPring-8," *Nucl. Instrum. Methods* A **616**(2-3), 237-240 (2010).

23. M. Thomasset and F. Polack, "Characterization of optical surfaces for the present generations of synchrotron sources," *Proc. SPIE* **7155**, 7155-06 (2008).

24. F. Polack, M. Thomasset, S. Brochet, A. Rommeveaux, "An LTP stitching procedure with compensation of instrument errors: Comparison of SOLEIL and ESRF results on strongly curved mirrors," *Nucl. Instrum Methods* A **616**(2-3), 207-211 (2010).

25. J. L. Kirschman, E. E. Domning, W. R. McKinney, G. Y. Morrison, B. V. Smith, and V. V. Yashchuk, "Performance of the upgraded LTP-II at the ALS Optical Metrology Laboratory," *Proc. SPIE* **7077**, 70770A (2008).

26. V. V. Yashchuk, "Optimal measurement strategies for effective suppression of drift errors," *Rev. Sci. Instrum.* **80**, 115101 (2009).

27. V. V. Yashchuk, S. Barber, E. E. Domning, J. L. Kirschman, G. Y. Morrison, B. V. Smith, F. Siewert, T. Zeschke, R. Geckeler, A. Just, "Sub-microradian surface slope metrology with the ALS Developmental Long Trace Profiler," *Nucl. Instrum. Methods* A **616**(2-3), 212-223 (2010).

28. O. Hignette, A. Freund, E. Chinchio, "Incoherent X-ray mirror surface metrology," *Proc. SPIE* **3152**, 188–99 (1997).

29. P. Mercère, M. Idir, J. Floriot, and X. Levecq, “Hartmann and Shack–Hartmann Wavefront Sensors for Sub-nanometric Metrology,” Chap. 15 in *Modern Developments in X-Ray and Neutron Optics*, A. Erko, M. Idir, T. Krist, and A. G. Michette, Eds., pp. 213-218, Springer, New York (2008).

30. K. A. Goldberg, P. Naulleau, P. Batson, P. Denham, H. Chapman, and J. Bokor, "Extreme ultraviolet alignment and testing of a four mirror aspheric extreme ultraviolet optical system," *J. Vac. Sci. Tech.* B **18**(6), 2911-15 (2000).

31. P. P. Naulleau, K. A. Goldberg and J. Bokor, "Extreme ultraviolet carrier-frequency shearing Interferometry of a lithographic four-mirror optical system," *J. Vac. Sci. Tech.* B **18**(6), 2939-43 (2000).

32. H. Yumoto, H. Mimura, S. Matsuyama, S. Handa, Y. Sano, M. Yabashi, Y. Nishino, K. Tamasaku, T. Ishikawa, and K. Yamauchi, “At-wavelength figure metrology of hard X-ray focusing mirrors,” *Rev. Sci. Instrum.* **77**(6), 063712 (2006).

33. W. R. McKinney, J. L. Kirschman, A. A. MacDowell, T. Warwick, V. V. Yashchuk, “Optimal tuning and calibration of bendable mirrors with slope measuring profilers,” *Opt. Eng.* **48**(8), 083601 (2009).

34. S. Yuan, V. V. Yashchuk, K. A. Goldberg, R. Celestre, W. R. McKinney, G. Morrison, T. Warwick, H. A. Padmore, “Development of in situ, at-wavelength metrology for soft x-ray nano-focusing,” *Nucl. Instrum. Methods* A **649**(1), 160-162 (2010).

35. E. L. Church, H. A. Jenkinson, and J. M. Zavada, “Relationship between surface scattering and micro-topographic features,” *Opt. Eng.* **18**(2), 125-136 (1979).

36. E. L. Church and H. C. Berry, “Spectral analysis of the finish of polished optical surfaces,” *Wear* **83**, 189-201 (1982).

37. J. C. Stover, *Optical Scattering*, 2nd ed., SPIE Optical Engineering Press, Bellingham (1995).

38. D. Attwood, *Soft X-rays and Extreme Ultraviolet Radiation*, Cambridge University Press, New York (1999).

39. Y.Z. Hu, K. Tonder, "Simulation of 3D random rough surface by 2D digital filter and Fourier analysis," *Int. J. Mach. Tools Manufact.* **32**, 83–90 (1992).

40. H. Yamaoka, T. Uruga, E. Arakawa, M. Matsuoka, Y. Ogasaka, K. Yamashita, N. Ohtomo, "Development and surface evaluation of large SiC x-ray mirrors for high-brilliance synchrotron radiation," *Japanese J. App. Phys*. **33**, 6718-6726 (1994).

41. J. Sherrington and G. W. Howarth, "Approximate numerical models of 3D surface topography generated using sparse frequency domain descriptions," *Int. J. Mach. Tools Manufact.* **38**(5-6), 599-606 (1998).

42. E. Sidick, "Power spectral density specification and analysis of large optical surfaces," *Proc. SPIE* **7390**, 73900L (2009).

43. V. L. Popova, and A. É. Filippov, "A model of mechanical polishing in the presence of a lubricant," *Tech. Phys. Lett.* **31**(9), 788–792 (2005).

44. A. V. Pret, R. Gronheid, T. Ishimoto, K. Sekiguchi, "Resist roughness evaluation and frequency analysis: metrological challenges and potential solutions for extreme ultraviolet lithography," *J. Micro/Nanolith. MEMS MOEMS* **9**(4), 041308 (2010).

45. F. Varnier, N. Mayani, G. Rasigni, and M. Rasigni, "Surface roughness for metallic thin films deposited upon various dielectric coatings," *J. Vac. Sci. Technol.* A **5**(4), 1806-1808 (1987).

46. M. H. Modi, S. K. Rai, M. Thomasset, G. S. Lodha, M. Idir, "Effect of surface roughness on multilayer film growth," *European Phys. J. – Spec. Topics* **167**, 27-32 (2009).

47. G. D. Boreman, *Modulation Transfer Function in Optical and Electro-optical Systems*, SPIE Press, Bellingham, Washington (2001).

48. J. M. Elson, J. M. Bennett, "Calculation of the power spectral density from surface profile data," *Appl. Opt.* **34**(1), 201-208 (2001).

49. R. Barakat, "Determination of the optical transfer function directly from the edge spread function," *J. Opt. Soc. Am.* **55**(10), 1217-1219 (1965).

50. B. Tatian, "Method for obtaining the transfer function from the edge response function," *J. Opt. Soc. Am.* **55**(8), 1014-1019 (1965).

51. O. P. Nijhawan, P. K. Datta, J. Bhushan, "On the measurement of MTF using periodic patters of rectangular and triangular wave-forms," *Nouv. Rev. Optique* **6**(1), 33-36 (1975).

52. K. Creath, "Calibration of numerical aperture effects in interferometric microscope objectives," *Appl. Opt.* **28**(15), 3333-3338 (1989).

53. P. Z. Takacs, M. X. Li, K. Furenlid, E. L. Church, "Step-height standard for surface-profiler calibration," *Proc. SPIE* **1995**, 235-244 (1993).

54. E. Levy, D. Peles, M. Opher-Lipson, and S. G. Lipson, "Modulation transfer function of a lens measured with a random target method," *Appl. Opt.* **38**(4), 679-683 (1999).

55. H. G. Rhee, T. V. Vorburger, J. W. Lee, and J. Fu, "Discrepancies between roughness measurements obtained with phase shifting interferometer and white-light interferometry," *Appl. Opt.* **44**(28), 5919-5927 (2005).

56. V. V. Yashchuk, A. D. Franck, S. C. Irick, M. R. Howells, A. A. MacDowell, W. R. McKinney, "Two dimensional power spectral density measurements of x-ray optics with the MicroMap interferometric microscope," *Proc. SPIE* **5858**, 58580A (2005).

57. V. V. Yashchuk, S. C. Irick, E. M. Gullikson, M. R. Howells, A. A. MacDowell, W. R. McKinney, F. Salmassi, T. Warwick, "Cross-check of different techniques for two dimensional power spectral density measurements of x-ray optics," *Proc. SPIE* **5921**, 59210G (2005).

58. V. V. Yashchuk, E. M. Gullikson, M. R. Howells, S. C. Irick, A. A. MacDowell, W. R. McKinney, F. Salmassi, T. Warwick, J. P. Metz, T. W. Tonnessen, "Surface roughness of stainless-steel mirrors for focusing soft x-rays," *Appl. Opt.* **45**(20), 4833-42 (2006).

59. J. Chu, Q. Wang, J. P. Lehan, G. Gao, and U. Griesmann, "Measuring the phase transfer function of a phase-shifting interferometer," *Proc. SPIE* **7064**, 70640C (2008).

60. J. Chu, Q. Wang, J. P. Lehan, G. Gao, and U. Griesmann, "Spatially resolved height response of phase-shifting interferometers measured using a patterned mirror with varying spatial frequency," *Opt. Eng.* **49**(9), 095601/1-7 (2010).

61. V. V. Yashchuk, W. R. McKinney, and P. Z. Takacs, "Binary Pseudorandom Grating Standard for Calibration of Surface Profilometers," *Opt. Eng.* **47**(7), 073602/1-5 (2008).

62. V. V. Yashchuk, W. R. McKinney, and P. Z. Takacs, "Binary Pseudorandom Grating as a Standard Test Surface for measurement of Modulation Transfer Function of Interferometric Microscopes," *Proc. SPIE* **6704**, 670408/1-12 (2007).

63. S. K. Barber, P. Soldate, E. D. Anderson, R. Cambie, W. R. McKinney, P. Z. Takacs, D. L. Voronov, and V. V. Yashchuk, "Development of Pseudo-random Binary Gratings and Arrays for Calibration of Surface Profile Metrology Tools*," J. Vac. Sci. and Tech.* B **27**(6), 3213-3219 (2009).

64. S. K. Barber, E. D. Anderson, R. Cambie, W. R. McKinney, P. Z. Takacs, J. C. Stover, D. L. Voronov, and V. V. Yashchuk, "Binary Pseudo-Random Gratings and Arrays for Calibration of

Modulation Transfer Function of Surface Profilometers," *Nucl. Instr. Methods* A **616**, 172-182 (2010).

65. V. V. Yashchuk, E. H. Anderson, S. K. Barber, N. Bouet, R. Cambie, R. Conley, W. R. McKinney, P. Z. Takacs, D. L. Voronov, "Calibration of the modulation transfer function of surface profilometers with binary pseudo-random test standards: expanding the application range to Fizeau interferometers and electron microscopes," *Opt. Eng.* **50**(9), 093604/1-12 (2011).
66. Shadow: Primier 2.0, http://www.esrf.eu/computing/scientific/raytracing/PDF/primer.pdf.
67. M. Sánchez del Río and A. Marcelli, "Waviness effects in ray-tracing of "real" optical surfaces," *Nucl. Instrum. Methods* A **319**(1-3), 170-177 (1997).
68. F. Schaefers, "RAY - the BESSY raytrace program to calculate synchrotron radiation beamlines," *Technischer Bericht*, BESSY TB **202**, 1-37 (1996).
69. F. Schäfers, "The BESSY ray trace program to calculate (not only) synchrotron radiation beamlines," http://www.esrf.eu/events/conferences/SMEXOS/talkSchaefers.
70. F. Schäfers, "The BESSY Raytrace Program RAY," Chap. 2 in *Modern Developments in X-Ray and Neutron Optics*, A. Erko, M. Idir, T. Krist, and A. G. Michette, Eds., pp. 9-41, Springer, New York (2008).
71. E. Knudsen, P. Willendrup, S. Schmidt, K. Lefmann, J. Baltser, A. Prodi, S. Kynde, K. Mortensen, "McXtrace - An X-ray Monte Carlo Ray-tracing software package," http://www.mcxtrace.org/images/f/fd/Mcxtrace-1.0_rc2-manual.pdf.
72. E. Knudsen, A. Prodi, P. Kjær Willendrup, and K. Lefmann, "User and Programmers Guide to the X-Ray-Tracing Package: McXtrace, Version 1.0 rc1," http://www.mcxtrace.org/images/f/fd/Mcxtrace-1.0_rc2-manual.pdf.

73. Here, we refer to the standard SHADOW software package. There are a number of SHADOW based developments with extended capabilities; see for example, M. S. del Rio, N. Canestrari, F. Jiang, and F. Cerrin, “SHADOW3: a new version of the synchrotron X-ray optics modeling package,” *J. Synchrotron Rad.* **18**, 708–716 (2011).
74. E. L. Church and P. Z. Takacs, “Specification of surface figure and finish in terms of system performance,” *App. Opt.* **32**(19), 3344-531 (1993).
75. E. L. Church and P. Z. Takacs, “Specification of glancing- and normal-incidence X-ray mirrors,” *Opt. Eng.* **34**(2), 353-60 (1995).
76. E. L. Church, “Fractal surface finish,” *App. Opt.* **27**(8), 1518-1526 (1988).
77. B. B. Mandelbrot, *The fractal geometry of nature*, Freeman, San Francisco (1977).
78. V. V. Yashchuk, E. L. Church, M. Howells, W. R. McKinney and P. Z. Takacs, "21st century metrology for synchrotron radiation optics - understanding how to specify and characterize optics," in The 3rd International Workshop on Metrology for X-ray Optics, Pohang Accelerator Laboratory, Daegu, Korea (2006).
79. P. Z. Takacs, S. Barber, E. L. Church, K. Kaznatcheev, W. R. McKinney, V. Y. Yashchuk, “2D Spatial Frequency Considerations in Comparing 1D Power Spectral Density Measurements,” Paper OWE5 in *Optical Fabrication and Testing*, OSA Technical Digest (CD), Optical Society of America (2010).
80. R. Soufli, M. J. Pivovaroff, S. L. Baker, J. C. Robinson, E. M. Gullikson, T. J. McCarville, P. M. Stefan, A. L. Aquila, J. Ayers, M. A. McKernan, R. M. Bionta, “Development, characterization and experimental performance of x-ray optics for the LCLS free-electron laser,” *Proc. SPIE* **7077**, 707716 (2008).

81. S. M. Kay, *Modern Spectral Estimation: Theory and Application*, Prentice Hall, Englewood Cliffs (1988).

82. V. V. Yashchuk, S. C. Irick, A. A. MacDowell, W. R. McKinney, P. Z. Takacs, "Air convection noise of pencil-beam interferometer for long-trace profiler," *Proc. SPIE* **6317**, 63170D (2006).

83. M. Yamauchi and K. Hibino, "Measurement of Air Turbulence for On-Machine Interferometry," *App. Opt.* **42**(34) 6869-6876 (2003).

84. G. M. Jenkins and D. G. Watts, *Spectral Analysis and its Applications*, 5th print., Emerson-Adams Press, Boca Raton (2007).

85. G. Rasigni, M. Lafraxo, V. Buat, M. Rasigni, F. Abdellani, and A. Llebaria, "Autoregressive process for characterizing statistically rough surfaces," *J. Opt. Soc. Am.* A **10**(6), 1257-1262 (1993).

86. B.-S. Chen, B.-K. Lee, and S.-C. Peng, "Maximum Likelihood Parameter Estimation of F-ARIMA Processes Using the Genetic Algorithm in the Frequency Domain," *IEEE Trans. on Signal Processing* **50**(9), 2208-2219 (2002).

87. S. Y. Chang and H-C. Wu, "Novel Fast Computation Algorithm of the Second-Order Statistics for Autoregressive Moving-Average Processes," *IEEE Trans. on Signal Processing* **57**(2), 526-535 (2009).

88. S. M. Pandit, P. T. Suratkar, and S. M. Wu, "Mathematical Model of a Ground Surface Profile with the Grinding Process as a Feedback System," *Wear* **39**(2), 205-12 (1976).

89. I. Fukumoto and T. Ayabe, "Improvement of Ground Surface Roughness in Al-Si Alloys," *Wear* **137**, 199-209 (1990).

90. G. Xinjian and H. Yiyljn, "The modeling and simulation of a rough surface," *Wear* **137**, 275 – 285 (1990).

91. E. Friot and R. Bouc, "Fast synthesis of ARMA for the recursive simulation of a scalar random process with a given target spectrum," *J. of Sound and Vibration* **179**(3), 415-421 (1994).

92. J.-J. Wu , "Simulation of rough surfaces with FFT," *Tribology International* **33**, 47–58 (2000).

93. P. M. T. Broersen and S. de Waele, "Generating data with prescribed power spectral density," *IEEE Trans. Instrum. and Meas.* **52**(4), 1061-1067 (2003).

94. *EViews 7 User's Guide*, Volumes I and II, Quantitative Micro Software, Irvine (2009); www.eviews.com.

95. A. Rommeveaux, M. Thomasset, D. Cocco, F. Siewert, "First report on a European round robin for slope measuring profilers," *Proc. SPIE* **5921**, 592101 (2005).

96. F. Siewert, L. Assoufid, D. Cocco, O. Hignette, S. Irick, H. Lammert, W. McKinney, H. Ohashi, F. Polack, S. Qian, S. Rah, A. Rommeveaux, V. Schönherr, G. Sostero, P. Takacs, M. Thomasset, K. Yamauchi, V. Yashchuk, T. Zeschke, in: CD Proceedings of the AIP Conference on Synchrotron Radiation Instrumentation SRI-2006, III Workshop on Optical Metrology, Daegu, South Korea, May 27 - June 03 (2006).

97. J. W. Allen, "Evaluation of the autoregression time-series model for analysis of a noisy signal," *Progress in Nucl. Energy* **1**, 603-613 (1977).

98. J.-C. Hung, A generic algorithm approach to the spectral estimation of time series with noise and missed observations, *Inform. Sci.* **178**, 4632-4643 (2008).

99. J. M. Wooldridge, *Introductory Econometrics: A Modern Approach*, 4th ed., South-Western Cengage Learning, Mason (2009).

100. A. Kizilkaya and A. H. Kayran, "Estimation of 2-D ARMA model parameters by using equivalent AR approach," *J. Franklin Inst.* **342**, 39-67 (2005).

AUTHOR BIOGRAPHIES

Yekaterina V. Yashchuk received her MA degree in Economics from the University of California at Santa Barbara in 2010. She worked at the Advanced Light Source, Lawrence Berkeley National Laboratory as a System Administrator on a short term project, using EViews econometics software to develop an analytical method for describing surface slope metrology of super polished X-ray optics and predicting the quality of the mirrors before ordering new optics. Currently, she is working at Esurance, Inc., in San Francisco as a Financial Planning Analyst.

Valeriy V. Yashchuk received his MS degree in experimental physics from St. Petersburg State University (Russia) in 1979, and his PhD degree from St. Petersburg Nuclear Physics Institute (Russia) in 1994. He is currently leading the Optical Metrology Laboratory at the Advanced Light Source, Lawrence Berkeley National Laboratory. He has authored more than 80 scientific articles in the fields of atomic and molecular physics, nonlinear optics, electro- and magneto-optics, laser spectroscopy, experimental scientific methods and instrumentation, and optical metrology. In 1986 for the development of a method of reduction of phase space of an atomic beam he was awarded the Leningrad Komsomol Prize in physics. In 2007, he received R&D Magazine's R&D 100 Award for development of Laser-Detected MRI. His current research interest is in x-ray optics, optical instrumentation and metrology for x-ray optics.

TABLES

Table 1: Parameters of the ARMA model (the red dashed line in Fig. 1a), which best fits the surface slope trace for the 1280 m radius spherical reference mirror measured with the ALS DLTP.[27] In Eqs. (4-8), $b_0 = 1$ and σ^2 is equal to the standard error (S.E.) of the regression. The data in the table are the regression outputs generated by EViews 7 software.

Dependent Variable: SLOPE
Method: Least Squares
Included observations: 543 after adjustments
Convergence achieved after 6 iterations

Variable	Coefficient	Std. Error	t-Statistic	Prob.
AR(1): a_1	1.118736	0.021838	51.22914	0.0000
AR(4): a_4	-0.145061	0.022404	-6.474687	0.0000
MA(2): b_2	0.299157	0.035204	8.497827	0.0000
MA(6): b_6	-0.171479	0.036455	-4.703891	0.0000
MA(3): b_3	0.093133	0.032904	2.830432	0.0048

R-squared	0.973238	Mean dependent variation	-0.016092
Adjusted R-squared	0.973039	S.D. dependent variation	0.443422
S.E. of regression	0.072809	Akaike info criterion	-2.392786
Sum squared residuals	2.852027	Schwarz criterion	-2.353218
Log likelihood	654.6415	Hannan-Quinn criterion	-2.377315
Durbin-Watson statistics	2.068010		

Table 2: Parameters of the ARMA model (the red dashed line in Fig. 5a) found for the generated slope trace. The generated trace is statistically identical to the surface slope trace measured with the 1280 m radius spherical reference mirror and discussed in Sec. 3. The data in the table are the regression outputs generated by EViews 7 software.

Dependent Variable: GSLOPE
Method: Least Squares
Included observations: 996 after adjustments
Convergence achieved after 5 iterations

Variable	Coefficient	Std. Error	t-Statistic	Prob.
AR(1): a_1	1.048968	0.018116	57.90297	0.0000
AR(4): a_4	-0.085087	0.018392	-4.626384	0.0000
MA(2): b_2	0.349078	0.026168	13.33998	0.0000
MA(6): b_6	-0.179654	0.025161	-7.140075	0.0000
MA(3): b_3	0.114945	0.022912	5.016748	0.0000

R-squared	0.967377	Mean dependent variation	-0.067029
Adjusted R-squared	0.967245	S.D. dependent variation	0.447451
S.E. of regression	0.080981	Akaike info criterion	-2.184192
Sum squared residuals	6.498934	Schwarz criterion	-2.159575
Log likelihood	1092.728	Hannan-Quinn criterion	-2.174834
Durbin-Watson statistics	2.015141		

FIGURE CAPTIONS

Figure 1: (a) Measured slope trace after subtracting the best-fitted spherical surface shape with a radius of curvature of 1287.5 m (the solid blue line); and best-fitted slope trace corresponding to the ARMA model specified in Table 1 (the red dashed line). The rms variation of the measured slope trace is 0.447 μrad. (b) Residual slopes equal to the difference between the measured and fitted traces in plots (a). The rms variation of the residual slope trace is 0.073 μrad. Note that the measured and the best-fitted traces are almost exactly overlapping.

Figure 2: Histogram normality test[94] for the residual slope of the regression shown in Fig. 1. (a) Histogram of the residuals. (b) Descriptive statistics of the residuals, including the Jarque-Bera statistic used for testing whether the residuals are normally distributed. All the descriptive statistics indicate that the residual slope is normally distributed.

Figure 3: Power spectral density distributions of the measured slope data (the solid blue curve) and the best-fitted ARMA model of the data (the dashed red curve). The corresponding straight lines depict the white-noise asymptotical behavior of the PSD distributions at the higher spatial frequencies.

Figure 4: ARMA analytical PSD calculated with the parameters given in Table 1 (the bold solid line) and two extreme ARMA predictions with increased (the dotted line) and decreased (the dashed line)

ARMA parameters; see text for details. For comparison, the DFT PSD spectrum of the measured slope trace is also shown with the solid blue curved line.

Figure 5: (a) Generated slope trace of 1000 points (the blue solid line) and the best-fitted slope trace (the red dashed line) corresponding to the ARMA model specified in Table 2. The rms variation of the generated slope trace of 0.447 μrad corresponds to the surface slope trace of the 1280 m radius spherical reference mirror (Fig. 1a). (b) Generated ARMA residuals with total number of 1000 points. The rms variation of the residual slope trace is 0.081 μrad. Note that the generated and the best-fitted traces are almost exactly overlapping.

Figure 6: DFT PSD spectrum of the generated slope trace (the blue solid curved line) and the ARMA analytical PSD calculated with the parameters given in Table 2 (the red bold solid line).